SELECTIVE DOLOMITIZATION BY SYNTAXIAL OVERGROWTH AROUND DETRITAL DOLOMITE NUCLEI: A CASE FROM THE JURASSIC OF THE LIGURIAN BRIANCONNAIS (LIGURIAN ALPS)

(Article begins on next page)

1
2
3
4
5   *This is an author version of the contribution published on*:
6   *Questa è la versione dell'autore dell'opera:*
7   *Journal of Sedimentary Research, vol. 84, 1, 2014, DOI: 10.2110/jsr.2014.2*
8
9   *The definitive version is available at:*
10   *La versione definitiva è disponibile alla URL:*
11   *http://www.sepm.org/pages.aspx?pageid=199*
12

SELECTIVE DOLOMITIZATION BY SYNTAXIAL OVERGROWTH

AROUND DETRITAL DOLOMITE NUCLEI: A CASE FROM THE

JURASSIC OF THE LIGURIAN BRIANÇONNAIS (LIGURIAN ALPS)

LUCA MARTIR E*[1], CARLO BERTOK[1], ANNA D'ATRI[1], ELENA PEROTTI[1], FABRIZIO PIANA[2]

luca.martire@unito.it

[1] *Dipartimento di Scienze della Terra, University of Torino, via Valperga Caluso 35, 10125 Torino, Italy*

[2] *Istituto di Geoscienze e Georisorse, Torino section, CNR, via Valperga Caluso 35, 10125 Torino, Italy*

Running title: SYNTAXIAL OVERGROWTH OF DETRITAL DOLOMITE

Key words: Detrital dolomite, syntaxial overgrowth, Jurassic, Ligurian Briançonnais, French-Italian Ligurian Alps.

ABSTRACT

Dolomite crystals, occurring in Middle Jurassic dolostones and dolomitic limestones of the Ligurian Briançonnais Domain (French-Italian Ligurian Alps), show irregular, complex zoning evidenced by cathodoluminescence (CL) and backscattered electron imaging. Comparable zoning patterns from other study areas have been attributed alternatively to recrystallization or dissolution-precipitation processes. However, none of these mechanisms can account for the range of observations from the Ligurian Briançonnais Domain, which include: 1) the presence of multiple core types, each with different CL characteristics; 2) marked compositional differences between cores and surrounding rims (ferroan vs. nonferroan, Mg/Ca ratio); 3) a marked shape difference between cores, with irregular outlines, and rims which progressively approach a well-developed rhombohedral habit. These features are most reasonably interpreted as dolomitic rims that formed as syntaxial overgrowths around detrital dolomite nuclei, which in turn originated from erosion of underlying Triassic rocks and triggered selective replacement of fine-grained calcareous sediment. Failure to recognize the exact nature of this type of dolomite crystal may lead to overestimating the degree of dolomitization and to overlooking possible detrital inputs in a basin otherwise supplied with pure allochemical sediments, with consequent loss of information on the tectonosedimentary evolution.

INTRODUCTION

The modes and environments of dolomitization of carbonate sediments are still an open and controversial problem in earth sciences. This ambiguity is due mainly to the fact that an actualistic approach seems to be largely inadequate, as the great abundance of dolomite in the geological past is at odds with its fairly rare occurrence in Holocene sediments (e.g., Hardie, 1987; Machel, 2004; Meister et al., 2013). The study of zoning in dolomite crystals provided important insights into dolomite formation mechanisms, showing that a number of processes, well known in limestone diagenesis, including recrystallization, dissolution, and void-filling cement precipitation, may be

57 common in dolostones too (e.g., Harris and Meyers, 1987; Cander et al., 1988; Gregg and Shelton,

58 1990; Gregg et al., 1993; Machel, 1997; Reinhold, 1998; Jones, 2005, 2007; Ehrenberg et al., 2006;

59 Choquette and Hiatt, 2008). Zoning refers to spatial differences of composition within a crystal

60 (Reeder, 1991) and, leaving aside sectoral zoning, may display a great variety of patterns: crystals

61 may be alternatively homogeneous (i.e., nonzoned), concentrically zoned with zone boundaries

62 parallel to crystal faces, concentrically zoned with irregular zone boundaries, or "chaotically zoned"

63 (i.e., displaying complex patchy distribution of compositionally different portions). Zoning reflects

64 changing conditions during crystal growth, from rapid growth in stable conditions, to steady state

65 growth under slightly changing chemical parameters, to more complex evolution of diagenetic

66 processes involving discontinuous growth, dissolution, and recrystallization. Cathodoluminescence,

67 because of its high sensitivity to minor geochemical changes in the diagenetic environment (e.g.,

68 activator and quencher concentration, Eh and pH, ion activity, growth rates; Machel and Burton,

69 1991; Machel, 2000), is a useful technique to highlight zoning. Cathodoluminescence moreover

70 allows identification of the most suitable portions of the crystals for carrying out further analyses

71 aimed at characterizing quantitatively the geochemical features of the different zones (e.g., Mg/Ca

72 ratios, Fe and Mn content, $\delta^{18}O$ and $\delta^{13}C$).

73 Studies on dolomitization, performed with this kind of petrographically controlled approach,

74 led recently to reinterpretations of previously described case histories. For example, Choquette and

75 Hiatt (2008) provided a new possible explanation of common fabrics in sucrosic dolostones such as

76 the so-called CCCR (cloudy-centered clear-rimmed dolomite: Murray, 1964; Sibley, 1982): they

77 showed that the cloudy cores consist of replacive dolomite, whereas clear rims consist of a

78 dolomite cement filling secondary pores generated by limestone dissolution. On the other hand,

79 dissolution of dolomite crystals followed by centripetal dolomite cementation in the resulting

80 hollows (inside-out dolomite: Jones 2007) has been proposed as an alternative hypothesis for

81 explaining complex zoning patterns that other authors related to recrystallization (Harris and

82 Meyers, 1987; Cander et al., 1988; Reinhold, 1998).

4

83   Complex zoning patterns have been recognized in dolomite contained in Middle Jurassic

84   dolomitic limestones of the Ligurian Briançonnais (Ligurian Alps, NW Italy) (Fig.1). Stratigraphic,

85   sedimentologic, petrographic, and geochemical evidence collectively indicate that none of the

86   above-mentioned processes can account for the observed pattern. This contribution does not discuss

87   all aspects of the dolomitization of the Jurassic limestones of the Ligurian Briançonnais; it is rather

88   focused on the description and interpretation of particular zoning patterns that may be of general

89   interest for researchers working on variably dolomitized strata. The purpose of this study is to

90   explore the possible importance of a different mechanism, a selective limestone replacement as

91   syntaxial overgrowths of dolomite around detrital grains.. The identification of this kind of dolomite

92   in fact documents the presence of terrigenous grains which otherwise could be unrecognized in

93   apparently pure allochemical rocks. This in turn may provide solid evidence of syndepositional

94   faulting that resulted in exhumation and erosion of older dolomitic formations. The diagenetic

95   evolution is also simplified as it changes from a complex sequence of events (dissolution,

96   reprecipitation, or recrystallization) to a single phase of dolomite growth around detrital cores.

97   Because it provides new insights, the syntaxially overgrown detrital dolomite (SODD) hypothesis

98   may be applicable to understanding other dolomites in the geologic record that do not find

99   satisfactory explanations in the existing models.

100

101   **GEOLOGICAL SETTING**

102   The Briançonnais Domain is one of the first-order tectonic units of the Alpine orogen (Fig.

103   1). It crops out from the Swiss Alps to the Ligurian Alps, where it is labelled "Ligurian

104   Briançonnais." In the frame of Alpine paleogeography, the Briançonnais has been interpreted as a

105   highstanding block, individuated during Late Triassic-Early Jurassic rifting, along the distal portion

106   of the European continental margin, bordering the western Tethys basin (Vanossi et al., 1984;

107   Lemoine et al., 1986; Lemoine and Trümpy, 1987; Lanteaume et al., 1990; Mohn et al., 2010).

108   Alpine deformation and metamorphism of the Briançonnais Domain generally decrease westward,

109   i.e., from the internal to the external parts. The study area is located in the exterior part (External

110   Ligurian Briançonnais)(Fig. 1), where deformation generated pervasive tectonic foliations confined

111   to marly and clayey intervals of the succession (Piana et al., 2009). Consequently, primary

112   stratigraphic features, such as depositional geometries, facies, and microfacies, are largely

113   preserved in carbonate sedimentary units.

114   The Ligurian Briançonnais consists of Permian volcanic and volcanosedimentary rocks

115   overlain by a Mesozoic-Cenozoic sedimentary succession that includes (Vanossi et al., 1984;

116   Lanteaume et al., 1990; Bertok et al., 2011) (Fig. 2): Upper Permian (?)-Lower Triassic

117   conglomerates and littoral cross-bedded quartz arenite (Quarziti di Ponte di Nava, QPN: over 100

118   m) overlain by Lower Triassic lagoonal mudrock 10-15 m thick (Peliti di Case Valmarenca, PCV);

119   Middle Triassic peritidal dolostone and dolomitic limestone (Dolomie di San Pietro dei Monti,

120   DSPM: about 300 m), bounded at the top by a Late Triassic to Middle Jurassic stratigraphic hiatus

121   caused by subaerial exposure; Middle Jurassic inner-shelf limestone and dolomitic limestone

122   (Calcari di Rio di Nava, CRN: 20-90 m); Upper Jurassic pelagic limestone, locally showing a Rosso

123   Ammonitico facies (Calcari di Val Tanarello, CVT: 10-60 m), bounded at the top by an important

124   stratigraphic discontinuity; Upper Cretaceous hemipelagic sediment (Formazione di Upega, FU:

125   about 100 m); Middle Eocene nummulite-rich limestone (Calcari della Madonna dei Cancelli,

126   CMC: about 30 m), overlying another unconformity and followed by hemipelagic and turbiditic

127   sediment (Flysch Noir, FN). Clear evidence of Middle Jurassic to Cretaceous post-rifting,

128   syndepositional tectonic activity, with extensional and transcurrent components, has recently been

129   documented in the study area (Bertok et al., 2011, 2012).

130

131   **MATERIALS AND METHODS**

132   This study is focused on the dolomite occurring in the Middle Jurassic CRN inner shelf

133   carbonates that range from almost pure dolostone to slightly dolomitic micritic limestone. Middle

134   Triassic dolomites have not been studied in detail, but only for purposes of comparison. Several

135   sections have been studied and sampled, spread over an area of about 10 km^2 (for location and

136   stratigraphy refer to Bertok et al., 2011). Petrographic studies of polished thin sections prepared

137   from about 30 specimens were carried out by plane-light, cross-polarized-light, and

138   cathodoluminescence (CL) microscopy, performed with CITL 8200 mk3 equipment (working

139   conditions: approximately 17 kV and 400 μA) to identify zoning in crystals. Backscattered electron

140   imaging (BSE) of polished thin sections was also carried out with a Cambridge Stereoscan 360

141   SEM instrument, which allowed differentiation between calcite and dolomite on a microscopic

142   scale, and, together with microprobe analyses, provided an opportunity to relate CL colors and

143   intensities to intracrystal compositional changes. Twenty seven *in situ* quantitative microprobe

144   analyses on dolomite crystals were performed with an EDS Energy 200 and a Pentafet detector

145   (Oxford Instruments) associated with the SEM. The operating conditions were: 15 kV accelerating

146   voltage, around 1 nA of probe current, and 50 seconds counting time. SEM-EDS quantitative data

147   (spot size = 2 μm) were acquired and processed using the Microanalysis Suite Issue 12, INCA Suite

148   version 4.01; SPI natural mineral standards were used to calibrate the raw data; the RoPhiZeta

149   correction (Pouchou and Pichoir, 1988) was applied. Analytical statistical errors Σ on atomic weight

150   % are 0.08 for Mg and Fe and 0.13 for Ca.

151

152   **DOLOMITE: OCCURRENCE AND FEATURES**

153   In the Mesozoic succession of the External Ligurian Briançonnais Domain, dolomite occurs

154   in the Middle Triassic DSPM and the Middle Jurassic CRN lithostratigraphic units. The DSPM

155   consists mainly of pure dolostones that exhibit different facies (mainly dolomicrite, massive or

156   thinly laminated, characterized by fenestrae or gypsum pseudomorphs, and subordinate peloidal

157   grainstone with flaser bedding and breccias) all reflective of a peritidal depositional environment.

158   These rocks mainly consist of very finely to finely crystalline dolomites (less than 10 μm to tens of

159   μm) resulting from a nondestructive replacement of micritic sediments. Very coarsely crystalline

160   dolomite (up to some millimeters) also occurs as a cement filling shrinkage pores and vugs.

161 Replacive dolomite displays CL colors ranging from nonluminescent (NL), to moderate to dull red

162 and greenish, depending on the beds (Fig. 3); void-filling dolomite cements displays moderate- to

163 bright-red colors. EDS analyses show that replacive dolomite consists of systematically nonferroan

164 and nearly stoichiometric dolomite (Ca:Mg molar ratio ranging from 1.0:1.0 to 1.05:0.95; low-Ca

165 calcian dolomite, LCD, of Jones and Luth, 2002)(N=4). Al_2O_3, SiO_2, and K_2O have also been

166 detected (total percentage around 2-3%) which point to the presence of a minor clay fraction.

167   Middle Jurassic CRN limestones show a variable degree of dolomitization that generally

168 decreases from the stratigraphic bottom to the top and that ranges from complete (at the very base in

169 one section, lowermost 50 cm) to only minor (less than about 5% dolomite in the uppermost part).

170 The most widespread limestone lithofacies consist of mudstone to wackestone with sparse crinoid

171 fragments and benthic foraminifera. Millimeter- to centimeter-size angular to rounded clasts of

172 dolostone occur at the very base as a transgressive lag over the Upper Triassic – Lower Jurassic

173 subaerial discontinuity surface. Single dolomite crystals, up to 200 μm in size, with a pitted,

174 irregular outline locally occur as nuclei of coated grains (ooids, microoncoids) in the matrix of such

175 transgressive conglomerate (Fig. 4). In some sections, angular to rounded, millimeter- to

176 centimeter-size clasts of dolostone also are present in the lower part of the Middle Jurassic

177 limestone, in centimeters- to decimeters-thick beds of matrix- to clast-supported breccia (Fig. 5).

178 The common occurrence of shrinkage pores in dolostone clasts documents their provenance from

179 the underlying Middle Triassic DSPM. Dolomite in pure dolostone at the very base of the CRN

180 occurs mainly as subhedral to euhedral crystals with planar faces (Fig. 3); crystal size is fairly

181 homogeneous, at approximately 100 μm. CL observations reveal that most dolomite crystals

182 contain irregularly shaped cores, mainly NL but also showing dull red and greenish luminescence.

183 The cores are surrounded by a thin bright orange rim. Scattered dull-blue-luminescing quartz grains

184 with the same size as dolomite crystals can also be recognized (Fig. 3)

185   Dolomite in CRN dolomitic limestone occurs as euhedral to subhedral crystals of variable

186 size (15 to 150 μm). They have irregularly shaped cores, 10 to 100 μm in size. Core edges are

187　generally highly irregular, angular, and with embayments, whereas planar edges and subrounded

188　shapes are uncommon (Figs. 6, 7, 8). Cores show the same CL features as those of the underlying

189　pure dolostone (mainly NL but also dull red and greenish) but are surrounded by more developed

190　and complexly zoned rims. The most common pattern is represented by an inner bright-orange

191　zone, directly surrounding the core, followed outward by a middle moderate-orange zone and by an

192　outer NL zone (Figs. 6, 7, 8). Local deviations from this common pattern include additional

193　discontinuous, bright-orange hairline zones. The markedly different colors enable clear observation

194　of the geometry of the interfaces between the different zones. Whereas cores display highly

195　irregular edges, with smooth to angular to very jagged outlines, outer zones tend to increasingly

196　approach the rhombic habit, so that each zone is thicker where the core edge was farther from the

197　rhomb faces. A quasi-perfect parallelism between zone interfaces and euhedral outer faces of the

198　crystal usually is reached only by the moderate-orange-NL boundary. The small size of the cores

199　and zoned rims commonly hinders accurate EDS analyses. However, where possible, analyses

200　reveal that NL nuclei and orange CL zones are nonferroan, whereas the NL outer zone is commonly

201　slightly ferroan ($0.7 - 2.0$ mole % $FeCO_3$). Moreover, the Ca:Mg ratio varies from 1.05:0.95 to

202　1.07:0.93 (average 1.06:0.94) in the cores (low-Ca calcian dolomite, LCD, of Jones and Luth, 2002)

203　(N=2) and from 1.08:0.92 to 1.19:0.81 in the rims (average 1.13:0.87, i.e., mostly high-Ca calcian

204　dolomite, HCD, of Jones and Luth, 2002) (N=11) (Fig. 9). BSE imaging also reveals zoning with

205　crystals exhibiting homogeneous, darker cores and lighter rims. Outer rims also are characterized by

206　brighter micrometer-size irregular spots composed of calcite (Fig. 10).

207　　　　Polycrystalline dolomite lithoclasts are also present; they are up to some hundred

208　micrometers in size and consist of decimicrometer-size crystals. They show a homogeneous

209　cathodoluminescence, which may be greenish, dull red, or NL, and are not surrounded by zoned

210　rims (Fig. 11). The Ca:Mg ratios (from 1.03:0.97 to 1.04:0.96) (N=2), nonferroan composition, CL

211　features, and presence of SiO_2 and Al_2O_3 allow comparison of these polycrystalline lithoclasts with

212　Triassic dolostone.

213   Dolomite also occurs as a coarsely crystalline mosaic, infilling a network of mainly

214   subvertical veins, up to 2 mm wide, which are locally developed. Veins crosscut the Middle Triassic

215   DSPM -Middle Jurassic CRN unit boundary and taper out, within some decimeters higher up in the

216   section, where the Jurassic strata display a gradual transition from fully dolomitized, at the base, to

217   partially dolomitized. A marked zoning of dolomite filling the veins is immediately apparent from

218   CL observation, with the following sequence (from inner to outer parts): I) NL, II) bright orange,

219   III) moderate orange, and IV) NL (Fig. 12). The two NL zones are ferroan ($1.7 – 3\%$ $FeCO_3$) (N=8)

220   whereas the orange luminescing zones are nonferroan as is also well evidenced by BSE images

221   (Fig. 12).

222

223   **DISCUSSION**

224   The features of dolomite observed in the Middle Jurassic carbonate rocks of the External

225   Ligurian Briançonnais Domain can be summarized as follows:

226   1) in the lower part of the CRN, lithoclastic breccia or conglomerate with dolostone clasts

227   are interbedded with micritic limestone. These beds have been interpreted as the result of storm-

228   induced currents transporting offshore clasts eroded from rocky coasts locally developed on Middle

229   Triassic, subaerially exposed, dolostone (Bertok et al., 2011);

230   2) monocrystalline dolomite grains occur as nuclei of coated grains in the lower part of the

231   CRN;

232   3) dolomite crystals are present throughout the CRN but are particularly abundant in the

233   lower part, where they are associated with quartz grains of comparable size and polycrystalline

234   dolomite lithoclasts up to some hundreds of micrometers in size;

235   4) dolomite crystals are zoned under CL and display homogeneous cores and zoned rims;

236   cores are irregularly shaped, whereas rims show increasingly better developed rhombohedral crystal

237   faces progressing outwards;

10

238   5) cores of dolomite crystals, occurring side by side in the same thin section, show a

239   conspicuous variability in CL features (NL, dull red, greenish);

240   6) independently of the size and CL color of the core, rims show the same succession of CL

241   zones;

242   7) vein-filling sparry dolomite mosaics show four CL zones (NL, bright orange, moderate

243   orange, NL), three of which (bright orange, moderate orange, NL) correlate with rims of rhombs;

244   8) polycrystalline dolomite lithoclasts are not surrounded by zoned rims;

245   9) compositional features (CL, BSE, Ca:Mg ratios, ferroan vs. nonferroan, presence or

246   absence of SiO_2 and Al_2O_3) show that cores are different from rims but indistinguishable from

247   Middle Triassic dolostones and polycrystalline clasts occurring in the lower part of the CRN.

248   Points 1 and 2 demonstrate that a dismantlement of Middle Triassic dolostone was taking

249   place in the Middle Jurassic during deposition of CRN. Finely crystalline dolostone gave rise to

250   polycrystalline lithoclasts of a size ranging from fine sand to pebbles. More coarsely crystalline

251   dolostone or fenestral pore-filling dolomite cements, instead, could weather out to monocrystalline

252   grains that were transported to a shallow marine environment where they acted as nuclei for coated

253   grains. Point 3 confirms that terrigenous grains were shed into the CRN basin and documents that

254   denudation and exposure affected also the Lower Triassic quartzarenites (QPN). Points 4, 5, and 6

255   document that the cores of dolomite crystals are primary elements of the Middle Jurassic sediment

256   whereas rims result from a common diagenetic evolution recorded by all dolomite rhombs. Point 7,

257   together with Point 4, proves that rims and vein-filling dolomite are coeval and cogenetical and that

258   rims grew outwards starting from the outer edges of cores. However, it is important to note that the

259   innermost zone of vein dolomite, which is NL, ferroan, and thus brighter in BSE, has no counterpart

260   in the rhombs and cannot be related to the NL cores (Figs. 9, 12, 13). Point 8 shows that

261   monocrystalline cores were necessary to trigger dolomite precipitation, which, conversely, did not

262   take place around fine-grained, polycrystalline lithoclasts. Point 9, together with Points 1, 2, 3, and

263   5, indicates that both polycrystalline clasts and dolomite crystal cores could be fragments of Middle

264   Triassic DSPM dolostone reworked into the Middle Jurassic CRN.

265   Detrital dolomite is not a novelty in the geological literature. It has been reported in a wide

266   array of stratigraphic and paleoenvironmental settings. The most obvious occurrence is in

267   terrigenous sediments whose source areas include carbonate successions (e.g., Ordovician non

268   marine sandstones, Texas: Amsbury 1962; Cretaceous coastal plain sandstones, Utah: Taylor et al

269   2000, 2004; Cretaceous glauconitic sandstones, Alberta: Young and Doig, 1986; Miocene

270   turbidites, Italian Apennines: Gandolfi et al., 1983). Dolomite grains found in mixed sediments

271   deposited in cool-water platforms (Plio-Pleistocene, Australia: Bone et al 1992, James and Bone

272   2007; Miocene, Menorca: Freeman et al., 1983) have a comparable origin. Carbonate successions

273   may include limited lithosomes of detrital dolomites interpreted as infillings of karstic cavities (e.g.,

274   Devonian, Canada: Morrow et al 1986; Ordovician, Virginia: Mussman and Read, 1986). Recent

275   deep-sea sediment also contains detrital-dolomite-rich beds that have been correlated to climatic

276   changes in turn affecting aridity, and thus eolian transport (e.g., Cullen et al 2000), or ice sheet

277   dynamics (Andrews and Tedesco, 1992; Knies et al., 1999; Ji et al 2009). Detrital dolomite was also

278   reported in ancient marine limestones and related to eolian transport of penecontemporaneous

279   dolomite from tidal flats or from the erosion of older carbonate rocks (Devonian, New York:

280   Lindholm, 1969; lower Palaeozoic, Newfoundland: Coniglio and James, 1988). The most

281   impressive report of a sedimentary body consisting almost entirely of terrigenous dolomite is the

282   Pennsylvanian Atoka Dolomite, several hundred meters thick, resulting from deposition in a fan-

283   delta environment of sediments eroded from Ordovician dolomites (Lyday, 1985). Many papers,

284   moreover, highlight the important role of detrital dolomite grains as nuclei for growth of authigenic

285   dolomite (Lindholm, 1969; Freeman et al., 1983; Bone et al 1992).

286   On the basis of the data and considerations reported above, it appears that the dolomite in

287   the Middle Jurassic CRN resulted from a process of replacement of calcareous sediment occurring

288   as selective overgrowth of authigenic syntaxial dolomite around silt- to sand-size, irregular,

289 monocrystalline grains of detrital dolomite (SODD: syntaxially overgrown detrital dolomite) (Fig.

290 13). These grains consist of clasts of reworked Middle Triassic DSPM dolostone showing non-, red

291 or greenish luminescence, depending on the stratigraphic level from where clasts were sourced. Silt-

292 to sand-size dolomitic detritus came from the same areas as the breccia-bed clasts, but it was finer

293 grained, scattered within Middle Jurassic sediment, and progressively decreasing in quantity going

294 up-section. The uppermost part of the Middle Triassic dolostones between the Late Triassic and the

295 Early Jurassic underwent a prolonged emersion that locally generated karstic cavities with terra

296 rossa infillings (e.g., Faure and Megard-Galli, 1988; Decarlis and Lualdi, 2008). The Middle

297 Jurassic sea consequently transgressed over rocky coasts made up of dolostones that had never been

298 deeply buried and thus were likely characterized by a typical intercrystalline porosity, possibly

299 enhanced by emersion-related dissolution. The mechanical action of shallow marine processes

300 (waves, storms etc.) led to the surficial disaggregation of these rocks, producing both coarse

301 polycrystalline clasts and finer-grained debris of single dolomite crystals whose external shape may

302 reflect the original euhedral outline, mechanical breakage, or chemical corrosion. The limited

303 degree of transport, probably mainly due to short-lived storm episodes (cf. Bertok et al., 2011),

304 accounts for the very low roundness of detrital cores.

305 The occurrence of detrital dolomite throughout the whole Middle Jurassic CRN, some tens

306 of meters thick, shows that the reworking of the Middle Triassic dolomites was not limited to the

307 earliest phase of transgression. This in turn implies that the Middle Jurassic transgression did not

308 take place over the top of a flat platform but affected a rugged topography that allowed the survival

309 of coastal or even emergent portions of the former Triassic platform. This is also confirmed by the

310 direct superposition of Upper Jurassic limestones over Middle Triassic dolostones in adjacent areas

311 (Vanossi, 1965) and by independent stratigraphic and sedimentologic evidence pointing to faulting

312 processes before and during CRN deposition (Bertok et al., 2011).

313 Detrital dolomite grains, now corresponding to the cores of zoned dolomite rhombs, acted as

314 nucleation sites for authigenic dolomite overgrowth. The widespread micrometer-size calcite

315 inclusions, very well imaged by BSE (Fig. 10) in the rims but absent in the cores, likely consist of

316 undolomitized portions of the original calcareous sediment, possibly corresponding to very fine-

317 grained fragments of skeletal grains.

318   At the base of the CRN succession, where detrital dolomite grains were closely packed, pure

319 dolostone were formed where the entire sequence of authigenic dolomite zones could not be

320 recorded; the latter were thicker and well developed in partially dolomitized mud-supported facies

321 with widely spaced dolomite grains. Each younger zone of authigenic dolomite contributed to

322 improve the outer crystal, habit increasingly approaching the rhombohedron that is almost perfectly

323 developed with the last, NL growth stage (Phases 3 and 4 in Fig. 13). This preferential growth

324 towards the rhombohedron edges, and in particular the acute ones, is reminiscent of the syntaxial

325 cements around echinoderm plates that grow at faster rates perpendicular to the plate edge i.e.,

326 along the c axis (e.g., Evamy and Shearman, 1965; Walkden and Berry, 1984).

327   The data also permit some thermodynamic inferences about the chemistry of the diagenetic

328 fluids flowing through these sediments (cf. Machel, 2004). The occurrence of a first NL ferroan

329 dolomite generation only within veins could be explained as the result of an early cementation

330 phase by fluids that were supersaturated with respect to dolomite but not undersaturated with

331 respect to calcite (phase 2 in Fig. 13). They therefore allowed precipitation of dolomite in open

332 fractures, but not replacement of calcareous sediments. Subsequently, fluids became undersaturated

333 with respect to calcite and only slightly supersaturated with respect to dolomite, so that dolomite

334 could precipitate by syntaxial overgrowth around a dolomite substrate. This substrate was provided

335 by detrital grains in sediments and by the first-stage dolomite crystals in veins.

336   Dolomite crystals with comparable zoning patterns have been commonly reported in the

337 literature. Basically, interpretations call upon recrystallization during burial (e.g., Harris and

338 Meyers, 1987; Cander et al., 1988; Reinhold, 1998), dissolution taking place during crystal growth

339 (e.g., Gregg et al., 1993), or intracrystalline dissolution of the core and precipitation of dolomite

340 cement in the resulting pore (inside-out dolomite: Jones, 2005, 2007).

341   In the case studied here, dolomite nuclei show a variety of CL emissions (NL, dull red,

342   greenish) and are surrounded by rims with the same dolomite CL stratigraphy (bright orange,

343   moderate orange, NL from the core outwards). The NL dolomite of the outer rim is a ferroan HCD

344   whereas that of the NL nuclei is a non ferroan LCD, i.e. ,they are compositionally very distinct.

345   Moreover, the variability in CL of the cores indicates that they cannot be interpreted as cements

346   filling intracrystalline voids formed by selective dissolution, unless several phases of very patchy

347   precipitation of dolomite cements with different CL are taken into account. Because such complex

348   process seems very unlikely and no evidence of dissolution is recognizable in the dolomite

349   lithoclasts, the inside-out model (Jones, 2007) cannot be applied to our case. Furthermore, the good

350   correlation of the CL zones bright orange, moderate orange, NL in core-surrounding rims from

351   rhombs to vein-filling dolomite definitely proves that rims grew outwards and confutes the inside-

352   out hypothesis that conversely would involve an inward growth of dolomite cement in a dissolution

353   cavity.

354   The absence of dissolution features, both in dolomite lithoclasts and in vein-filling dolomite

355   where CL zones are separated by perfectly planar boundaries (Fig. 10), is a valid argument to

356   exclude the possibility of an interruption in crystal growth, associated with some dissolution, and

357   followed by renewed precipitation over a pitted surface, as proposed by Gregg et al. (1993). The

358   shape of the surfaces separating rim dolomite zones (bright orange, moderate orange, NL), roughly

359   subparallel to core edges and developing increasingly euhedral habits progressing outwards, further

360   supports this conclusion and allows to rule out also the hypothesis of recrystallization (Harris and

361   Meyers, 1987; Cander et al., 1988; Reinhold, 1998). The latter would have produced a more

362   chaotic, patchy, luminescence.

363   The recognition that zoned dolomite crystals may be due to diagenetic overgrowth around

364   inherited, detrital grains goes beyond the mere petrographic aspect and involves wider geological

365   implications. The most relevant conclusion of general interest of this study is that dolomite crystals

366   showing the features here described are *per se* evidence of the presence of detrital grains of

367 extrabasinal origin. This may be trivial in terrigenous or mixed sediments but is of utmost

368 importance in presumably pure allochemical rocks, such as dolostones or dolomitic limestones, in

369 which the growth of diagenetic dolomite masks the presence of a pristine inherited clastic

370 component. If dolomitic formations occur stratigraphically below the SODD-bearing rocks, as in

371 the present case study, some kind of faulting leading to superficial exposure and erosion of

372 previously buried rocks is documented. If instead there is no dolomitic body in the local

373 stratigraphy, the source of the detrital dolomite cores should be searched in allochthonous terranes.

374 In both cases recognition of SODD may provide an additional or even unique clue to

375 syndepositional tectonics.

376   The second conclusion refers to the diagenetic evolution. The hypothesis here proposed of

377 syntaxially overgrown detrital dolomite implies only a single phase of dolomite precipitation

378 whereas other models, calling upon dissolution, reprecipitation, or recrystallization, involve a more

379 complex diagenetic evolution with obvious implications over patterns of fluid flow through

380 sedimentary-basin infills.

381   Moreover, the SODD hypothesis imposes a re-evaluation of the actual degree of

382 dolomitization in dolomitic limestones and dolostones since only the overgrowths could be due to

383 calcite replacement. In principle, some dolostones could consist mostly of detrital dolomite, with

384 authigenic dolomite representing only a minor part of the whole rock volume, as it has indeed been

385 reported already in literature (e.g., Lyday, 1985).

386   Lastly, this study shows that dolomitization may be very selective and it may take place only

387 around detrital dolomite grains. It is worth highlighting that in the absence of such clasts no

388 dolomitization takes place and the flow of potentially dolomitizing fluids leaves no evidence.

389 On the basis of what is discussed above, the main difference of this paper with respect to the one by

390 Choquette and Hiatt (2008), which treats a similar topic, concerns the implications. The major

391 conclusion by Choquette and Hiatt (2008) is that a significant part of sucrosic dolostones results

392 from free-space cementation and not replacement. The detrital origin of dolomite cores was just

393 hypothesized, as a possible alternative to an authigenic origin, due to their small size, substantially

394 of a few micrometers, making them not easily visible in thin section. In the case described in the

395 present paper, dolomite cores commonly reach a fine-sand grain size, give rise to a complex zoning

396 of dolomite rhombs which is perfectly recognizable in thin section, and represent a significant

397 portion of the whole dolomite volume. Therefore, the focus here lies in the proposal of a further

398 model for explaining irregularly zoned dolomite rhombs that adds to the existing ones involving

399 dissolution during growth, dissolution after full rhomb growth, and recementation, or

400 recrystallization.

401

402 **CONCLUSIONS**

403   - Stratigraphic, sedimentologic, petrographic, and geochemical evidence from the Middle

404 Jurassic CRN dolomitic limestone and dolostone of the Ligurian Briançonnais Domain (French-

405 Italian Ligurian Alps) document that irregularly zoned dolomite crystals consist of two distinct

406 domains: an irregularly shaped core of detrital origin and an authigenic rim related to

407 postdepositional diagenesis.

408   - Dolomite cores originated as the monocrystalline component of a detrital input that

409 included also polycrystalline clasts ranging in size from fine sand to pebbles. They were eroded

410 from exposed portions of Middle Triassic dolostone and delivered to the shallow marine CRN

411 basin.

412   - Dolomitization of Middle Jurassic CRN limestone was very selective and proceeded only

413 around the irregular fragments of detrital dolomite grains, giving rise to syntaxial overgrowths.

414   - Dolomite overgrowth around detrital cores provides another possible explanation for

415 irregularly zoned dolomite rhombs in addition to dissolution, reprecipitation, or recrystallization. In

416 spite of a great deal of research on dolomitization, such a process has not been kept in due

417 consideration so far. Although more than forty years have passed, a statement by Lindholm (1969)

418 seems to be still a very living issue: "The role of detrital dolomite in carbonate sedimentation and

419 diagenesis warrants attention in future works." Actually not all dolomite in a dolomite-bearing

420 carbonate rock may be due to dolomitization.

421   - The recognition of SODD documents the presence of terrigenous grains which otherwise

422 could be unrecognized in apparently pure allochemical rocks. It may also provide indirect evidence

423 of syndepositional tectonics resulting in fault-related exhumation of previously buried formations or

424 even the emplacement of allochthonous units.

425

426

433

434   **REFERENCES**

435 AMSBURY, D.L., 1962, Detrital dolomite in Central Texas: Journal of Sedimentary Petrology, v. 32,

436   p. 5−14.

437 ANDREWS, J.T., AND TEDESCO, K., 1992, Detrital carbonate-rich sediments, northwestern Labrador

438   Sea: implications for ice-sheet dynamics and iceberg rafting (Heinrich) events in the North

439   Atlantic: Geology, v. 20, p. 1087−1090.

440 BERTOK, C., MARTIRE, L., PEROTTI, E., d'ATRI, A., AND PIANA, F., 2011, Middle-Late Jurassic

441   syndepositional tectonics recorded in the Ligurian Briançonnais succession (Marguareis–

442   Mongioie area, Ligurian Alps, NW Italy): Swiss Journal of Geosciences, v. 104, p. 237–255.

443 BERTOK, C., MARTIRE, L., PEROTTI, E., D'ATRI, A., AND PIANA, F., 2012, Kilometre-scale

444   palaeoescarpments as evidence for Cretaceous synsedimentary tectonics in the External

445   Briançonnais Domain (Ligurian Alps, Italy): Sedimentary Geology, v. 251-252, p. 58–75.

446 BIGI, G., COSENTINO, D., PAROTTO, M., SARTORI, R., AND SCANDONE, P., 1990, Structural Model

447   of Italy 1:500000, sheet 1: Firenze, SELCA.

448 BONE, Y., JAMES, N.P., AND KYSER, T.K., 1992, Synsedimentary detrital dolomite in Quaternary

449   cool-water carbonate sediments, Lacepede shelf, South Australia, Geology, v. 20, p. 109−112.

450 CANDER, H.S., KAUFMAN, J., DANIELS, L.D., AND MEYERS, W.J., 1988, Regional dolomitization of

451   shelf carbonates in the Burlington-Keokuk Formation (Mississippian), Illinois and Missouri:

452   constraints from cathodoluminescent zonal stratigraphy, *in* Shukla, V., and Baker, P.A., eds.,

453   Sedimentology and Geochemistry of Dolostones: SEPM, Special Publication 43, p. 129−144.

454 CHOQUETTE, P.W., AND HIATT, E.E., 2008, Shallow-burial dolomite cement: a major component of

455   many ancient sucrosic dolomites: Sedimentology, v. 55, p. 423−460.

456 CONIGLIO, M., AND JAMES, N.P:, 1988, Dolomitization of deep-water sediments, Cow Head Group

457   (Cambro-Ordovician), western Newfoundland, Journal of Sedimentary Petrology, v. 58, p.

458   1032−1045.

459 CULLEN, H.M., DEMENOCAL, P.B., HEMMING, S., HEMMING, G., BROWN, F.H., GUILDERSON, T., AND

460   SIROCKO, F., 2000, Climate change and the collapse of the Akkadian empire: evidence from the

461   deep sea: Geology, v. 28, p. 379−382.

462 DECARLIS, A., AND LUALDI, A., 2008, Late Triassic-Early Jurassic paleokarst from the Ligurian Alps

463   and its geological significance (Siderolitico Auct., Ligurian Briançonnais domain): Swiss

464   Journal of Geosciences, v. 101, p. 579–593.

465 EHRENBERG, S.N., MCARTHUR, J.M., AND THIRLWALL, M.F., 2006, Growth, demise, and

466   dolomitization of Miocene carbonate platforms on the Marion Plateau, offshore NE Australia:

467   Journal of Sedimentary Research, v. 76, p. 91−116.

468 EVAMY, B.D., AND SHEARMAN, D.J., 1965, The development of overgrowths from echinoderm

469   fragments: Sedimentology, v. 5, p. 211−233.

470 FAURE, J. L., AND MEGARD-GALLI, J., 1988, L'émersion jurassique en Briançonnais: sédimentation

471   continentale et fracturation distensive: Société Géologique de France, Bulletin, v. 4, p. 681–

472   692.

473 FREEMAN, T., ROTHBARD, D., AND OBRADOR, A., 1983, Terrigenous dolomite in the Miocene of

474   Menorca (Spain): provenance and diagenesis, Journal of Sedimentary Petrology, v. 53, p.

475   543−548.

476 GANDOLFI, G., PAGANELLI, L., AND ZUFFA, G.G., 1983, Petrology and dispersal pattern in the

477   Marnoso-Arenacea Formation (Miocene, Northern Apennines), Journal of Sedimentary

478   Petrology, v. 53, p. 493−507.

479 GREGG, J.M., AND SHELTON, K.L, 1990, Dolomitization and dolomite neomorphism in the back reef

480   facies of the Bonneterre and Davis Formations (Cambrian), southeastern Missouri. Journal of

481   Sedimentary Petrology, v. 60, p. 549−562.

482 GREGG, J.M., LAUDON, P.R., WOODY, R.E., AND SHELTON, K.L., 1993, Porosity evolution of the

483   Cambrian Bonneterre Dolomite, south-eastern Missouri, USA: Sedimentology, v. 40, p.

484   1153−1169.

485 HARDIE, L.A., 1987, Dolomitization: a critical view of some current views: Journal of Sedimentary

486   Petrology, v. 57, p. 166−183.

487 HARRIS, D.C., AND MEYERS, W.J., 1987, Regional dolomitization of subidal shelf carbonates:

488   Burlington and Keokuk Formations (Mississippian), Iowa and Illinois, *in* Marshall, J.D., ed.,

489   Diagenesis of Sedimentary Sequences: Geological Society of London, Special Publication 36,

490   p. 237−258.

491 JAMES, N.P., AND BONE, Y., 2007, A Late Pliocene–Early Pleistocene, inner-shelf, subtropical,

492   seagrass-dominated carbonate: Roe Calcarenite, Great Australian Bight, Western Australia:

493   Palaios, v. 22, p. 343−359.

494   JI, J., GE, Y., BALSAM, W., DAMUTH, J.E., AND CHEN, J., 2009, Rapid identification of dolomite

495   using a Fourier Transform Infrared Spectrophotometer (FTIR): a fast method for identifying

496   Heinrich events in IODP Site U1308: Marine Geology, v. 258, p. 60−68.

497   JONES, B., 2005, Dolomite crystal architecture: genetic implications for the origin of the Tertiary

498   dolostones of the Cayman Islands: Journal of Sedimentary Research, v. 75, p. 177−189.

499   JONES, B., 2007, Inside-out dolomite: Journal of Sedimentary Research, v. 77, p. 539−551.

500   JONES, B., AND LUTH, R.W., 2002, Dolostones from Grand Cayman, Bristish West Indies: Journal

501   of Sedimentary Research, v. 72, p. 560−570.

502   KNIES, J., VOGT, C., AND STEIN, R., 1999, Late Quaternary growth and decay of the

503   Svalbard/Barents Sea ice sheet and paleoceanographic evolution in the adjacent Arctic Ocean:

504   Geo-Marine Letters, v. 18, p. 195−202.

505   LANTEAUME, M., RADULESCU, N., GRAVOS, M., FERAUD, J., 1990, Notice explicative, Carte

506   Géologique de France (1/50.000), feuille Viève-Tende (948): Orléans, Bureau de Recherches

507   Géologiques et Minières, 139 p.

508   LEMOINE, M., BAS, T., ARNAUD-VANNEAU, A., ARNAUD, H., DUMONT, T., GIDON, M., BOURBON,

509   M., DEGRACIANSKY, P.C., RUDKIEWICZ, J.L., MEGARD-GALLI, J., AND TRICART, P., 1986, The

510   continental margin of the Mesozoic Tethys in the Western Alps: Marine and Petroleum

511   Geology, v. 3, p. 179–199.

512   LEMOINE, M., AND TRÜMPY, R., 1987, Pre-oceanic rifting in the Alps: Tectonophysics, v. 133, p.

513   305−320.

514   LINDHOLM, R.C., 1969, Detrital dolomite in Onondaga limestone (Middle Devonian) of New York:

515   its implications to the "Dolomite question": American Association of Petroleum Geologists,

516   Bulletin, v. 53, p. 1035−1042.

517   LYDAY, J.R., 1985, Atokan (Pennsylvanian) Berlin Field: genesis of recycled detrital dolomite

518   reservoir, deep Anadarko Basin, Oklahoma: American Association of Petroleum Geologists,

519   Bulletin, v. 69, p. 1931−1949.

520   MACHEL, H.G., 1997, Recrystallization versus neomorphism, and the concept of significant

521   recrystallization in dolomite research: Sedimentary Geology, v. 113, p. 161−168.

522   MACHEL, H.G., 2000, Applications of cathodoluminescence to carbonate diagenesis, *in* Pagel, M.,

523   Barbin, V., Blanc, P., and Ohnenstetter, D., eds., Cathodoluminescence in geosciences: New

524   York, Springer, p. 271−301.

525   MACHEL, H.G., 2004, Concepts and models of dolomitization: a critical reappraisal, *in* Braithwaite,

526   C.J.R., Rizzi, G., and Darke, G., eds., The Geometry and Petrogenesis of Dolomite

527   Hydrocarbon Reservoirs: Geological Society of London, Special Publication 235, p. 7−63.

528   MACHEL, H.G., AND BURTON, E.A., 1991, Factors governing cathodoluminescence in calcite and

529   dolomite and their implications for studies of carbonate diagenesis, *in* Barker, C.E., and KOPP,

530   O.C., eds., Luminescence Microscopy and Spectroscopy: Qualitative and Quantitative

531   Applications: SEPM, Short Course 25, p. 37−57.

532   MEISTER, P., MCKENZIE, J.A., BERNASCONI, S.M., AND BRACK, P., 2013, Dolomite formation in the

533   shallow seas of the Alpine Triassic: Sedimentology, v. 60, p. 270−291.

534   MOHN, G., MANATSCHAL, G., MÜNTENER, O., BELTRANDO, M., AND MASINI, E., 2010, Unravelling

535   the interaction between tectonic and sedimentary processes during lithospheric thinning in the

536   Alpine Tethys margins: International Journal of Earth Sciences, v. 99, p. 75−101.

537   MORROW, D.W., CUMMING, G.L., AND KOEPNICK, R.B., 1986, Manetoe facies – a gas-bearing,

538   megacrystalline, Devonian dolomite, Yukon and Northwest territories, Canada: American

539   Association of Petroleum Geologists, Bulletin, v. 70, p. 702−720.

540   MURRAY, R.C., 1964, The origin of porosity in carbonate rocks, *in* Imbrie, J., and Newell, N., eds.,

541   Approaches to Palaeoecology: New York, John Wiley, p. 388−403.

542   MUSSMAN, W.J, AND READ, J.F., 1986, Sedimentology and development of a passive- to

543   convergent-margin unconformity: Middle Ordovician Knox unconformity, Virginia

544   Appalachians, Geological Society of America, Bulletin, v. 97, p. 282−295.

545   PIANA, F., MUSSO, A., BERTOK, C., D'ATRI, A., MARTIRE, L., PEROTTI, E., VARRONE, D., AND

546   MARTINOTTI, G., 2009, New data on post-Eocene tectonic evolution of the External Ligurian

547   Briançonnais (Western Ligurian Alps): Italian Journal of Geosciences, v. 128, p. 353−366.

548   POUCHOU, J.L., AND PICHOIR, F., 1988, Determination of mass absorption coefficients for soft X-

549   rays by use of the electron microprobe, *in* Newbury, D.E., ed., Microbeam Analysis: San

550   Francisco: San Francisco Press, p. 319−324.

551   REEDER, R.J., 1991, An overview of zoning in carbonate minerals, *in* Barker, C.E., and Kopp, O.C.,

552   eds., Luminescence Microscopy and Spectroscopy: Qualitative and Quantitative Applications:

553   SEPM, Short Course 25, p. 77−82.

554   REINHOLD, C., 1998, Multiple episodes of dolomitization and dolomite recrystallization during

555   shallow burial in Upper Jurassic shelf carbonates: eastern Swabian Alb, southern Germany:

556   Sedimentary Geology, v. 121, p. 71−95.

557   SIBLEY, D.F., 1982, The origin of common dolomite fabrics: clues from the Pliocene: Journal of

558   Sedimentary Petrology, v. 52, p. 1087−1100.

559   TAYLOR, K.G., GAWTHORPE, R.L., CURTIS, C.D., MARSHALL, J.D., AND AWWILLER, D.N., 2000,

560   Carbonate cementation in a sequence-stratigraphic framework: Upper Cretaceous sandstones,

561   Book Cliffs, Utah–Colorado: Journal of Sedimentary Research, v. 70, p. 360–372.

562   TAYLOR, K.G., GAWTHORPE, R.L., AND FANNON-HOWELL, S., 2004, Basin-scale diagenetic

563   alteration of shoreface sandstones in the Upper Cretaceous Spring Canyon and Aberdeen

564   Members, Blackhawk Formation, Book Cliffs, Utah: Sedimentary Geology, v. 172, p. 99−115.

565   VANOSSI, M., 1965, Le unità stratigrafico-strutturali tra il Pizzo di Ormea e il Monte Galero (Alpi

566   Marittime): Università di Pavia, Istituto Geologico, Atti, v. 16, p. 114−184.

567   VANOSSI, M., CORTESOGNO, L., GALBIATI, B., MESSIGA, B., PICCARDO, G., AND VANNUCCI, R.,

568   1984, Geologia delle alpi liguri: dati, problemi, ipotesi: Società Geologica Italiana, Memorie, v.

569   28, p. 5–75.

570 WALKDEN, G.M., AND BERRY, J.R., 1984, Natural calcite in cathodoluminescence: crystal growth

571   during diagenesis: Nature, v. 308, p. 525−527.

572 YOUNG, H.R., AND DOIG, D.J., 1986, Petrography and provenance of the glauconitic sandstone,

573   South-Central Alberta, with comments on the occurrence of detrital dolomite: Bulletin of

574   Canadian Petroleum Geology, v. 34, p. 408−425.

575

576

577 **FIGURE CAPTIONS**

578 Figure 1. Simplified geological map with the main tectonostratigraphic units and domains of the

579 southwestern portion of the Alps. The black square indicates the study area. (Redrawn after Bigi et

580 al., 1990).

581 Figure 2. Log of the stratigraphic succession of the study area. QPN Quarziti di Ponte di Nava

582 (quartzarenite); PCV Peliti di Case Valmarenca (mudrock); DSPM Dolomie di S. Pietro dei Monti

583 (dolostone and dolomitic limestone); CRN Calcari di Rio di Nava (limestone and dolomitic

584 limestone); CVT Calcari di Val Tanarello (pelagic limestone); FU Formazione di Upega (marly

585 limestone); CMC Calcari della Madonna dei Cancelli (nummulite-rich limestone); FN Flysch Noir

586 (interbedded mudrock and sandstone).

587 Figure 3. A) Transmitted-light photomicrograph and B) CL image showing the stratigraphic

588 boundary between the Middle Triassic DSPM and the overlying the Middle Jurassic CRN. Note: the

589 greenish luminescence of the very finely to finely crystalline DSPM dolostones (compare with

590 Figure 11); the coarser size of the subhedral to euhedral dolomite crystals in the CRN, composed of

591 irregular cores with different luminescences (NL, dull red) surrounded by a thin bright orange rim;

592 the occurrence of dull blue luminescing quartz grains.

593

594 Figure 4. Transmitted-light photomicrograph showing a grainstone as the matrix of the

595 transgressive conglomerate locally occurring at the base of the Middle Jurassic CRN and including

596   lithoclasts of Middle Triassic DSPM: note a dolomite crystal with a pitted edge at the core of a

597   coated grain.

598

599   Figure 5: Clast- to matrix-supported breccia bed with angular to rounded clasts made of light

600   Middle Triassic DSPM interbedded with micritic limestone in the lower part of the Middle Jurassic

601   CRN. Tip of pencil at the bottom for scale is 7 cm long.

602

603   Figure 6. A) Transmitted-light photomicrograph of a partly dolomitized Middle Jurassic CRN

604   micritic limestone. The white square indicates the CL close up of Fig. 6B. B) CL image of the

605   squared area in Part A. Note: the commonly euhedral habit of dolomite crystals; the internal zoning;

606   the irregular shape of the nonluminescent cores. For further details see text.

607

608   Figure 7. A) Transmitted light photomicrograph and B) CL image of a partly dolomitized Middle

609   Jurassic CRN micritic limestone. Note in the CL image the differently luminescing cores of

610   dolomite crystals, ranging from NL to dull red to greenish.

611

612   Figure 8. A) Transmitted light photomicrograph and B) CL image of a partly dolomitized Middle

613   Jurassic CRN micritic limestone. Note in the CL image the differently luminescing cores of

614   dolomite crystals, ranging from NL to moderate red.

615

616   Figure 9. Sketch summarizing the main features of the different zones of dolomite rhombs. Ca:Mg

617   ratios are average values. Among the three possibilities of CL colors of the cores (NL, red and

618   greenish), the green one has been chosen not to make confusion with the red or NL color of rim

619   zones.

620

621 Figure 10. BSE image of a partly dolomitized Middle Jurassic CRN limestone. Note: the contrast

622 between the homogeneous core and the outer rims spotted with brighter micrometer-size calcite; the

623 lighter color of rims compared to that of the core, related to higher amounts of Ca in dolomite.

624

625 Figure 11. A) Transmitted-light photomicrograph and B) CL image of a partly dolomitized Middle

626 Jurassic CRN micritic limestone. The CL image shows the greenish luminescence of a finely

627 crystalline lithoclast of Middle Triassic DSPM (compare with Fig. 3).

628

629 Figure 12. A) Transmitted-light photomicrograph, B) CL image, and C) BSE image of a dolomite-

630 filled vein crosscutting the finely crystalline Middle Triassic DSPM dolostones. The white square in

631 Part B indicates the BSE close-up of Part C. In the CL image, four growth zones (I to IV) of

632 dolomite cement are clearly evidenced by NL, bright orange, moderate orange and NL

633 luminescence. In the BSE image the higher Fe content of zones I and IV is evidenced by lighter

634 colors.

635

636 Figure 13. Cartoon sketching the main phases (1 to 4) of formation of the dolomite. Detrital

637 fragments of dolomite (in green) are deposited together with carbonate mud in Middle Jurassic

638 limestone (1). A first generation of NL dolomite (in black) precipitates only as cement in fractures

639 (2). The subsequent flow of fluids undersaturated in calcite and slightly supersaturated in dolomite

640 results in formation of the same dolomite zones (in bright red, moderate red and dark grey) both in

641 veins and as syntaxial overgrowths around detrital cores (3-4).

642

643

644

645

646   Fig. 1

647

648

649

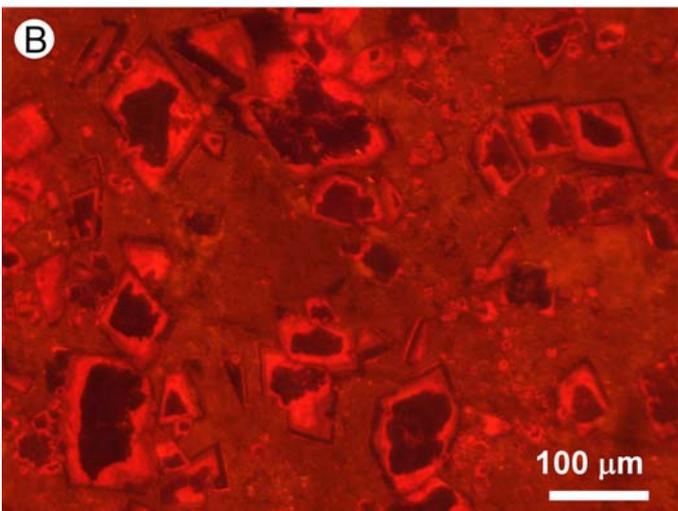650

651   Fig. 2

652

653

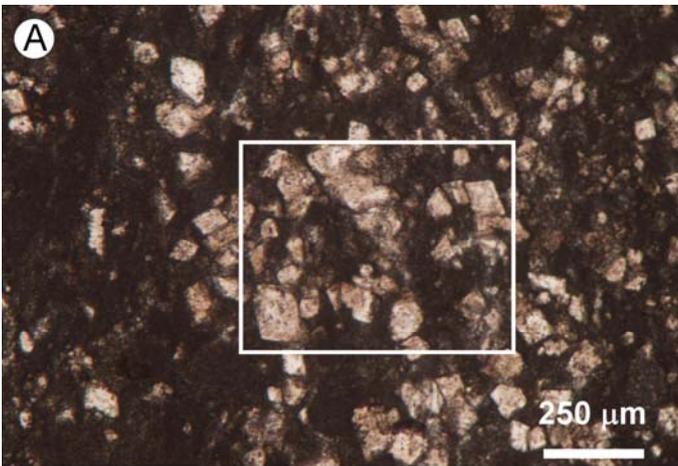654   Fig. 3

655

656

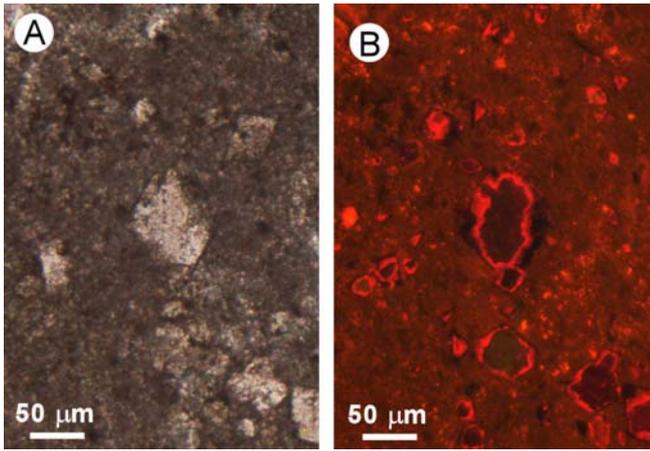657   Fig. 4

658

659

660   Fig. 5
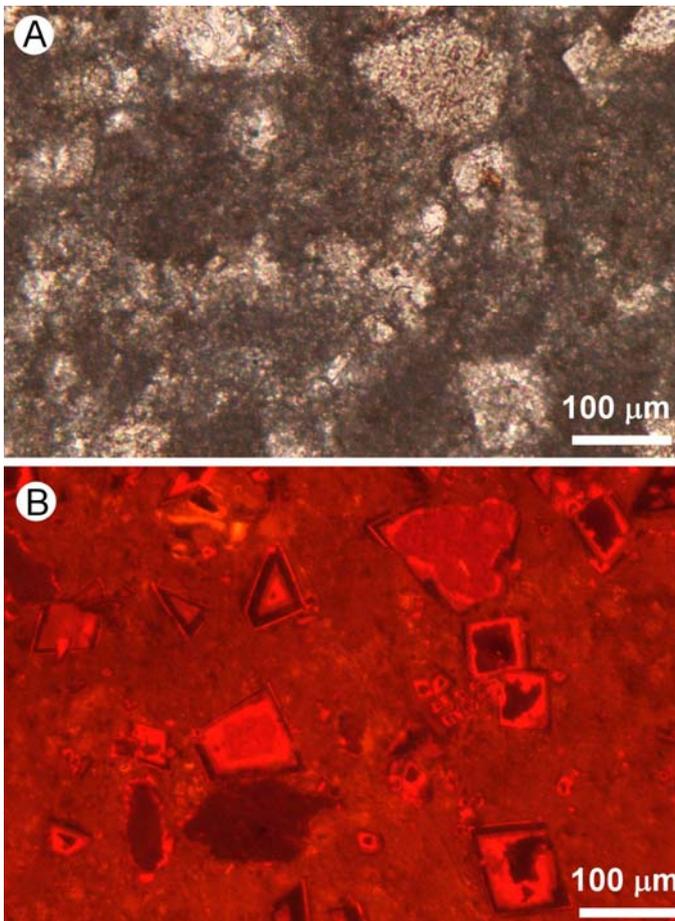
661

662

663

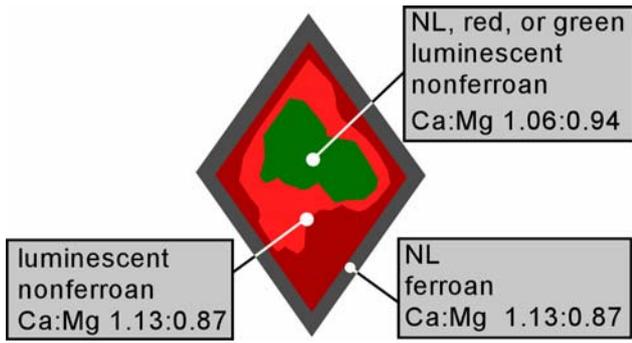664   Fig. 6

665

666

667

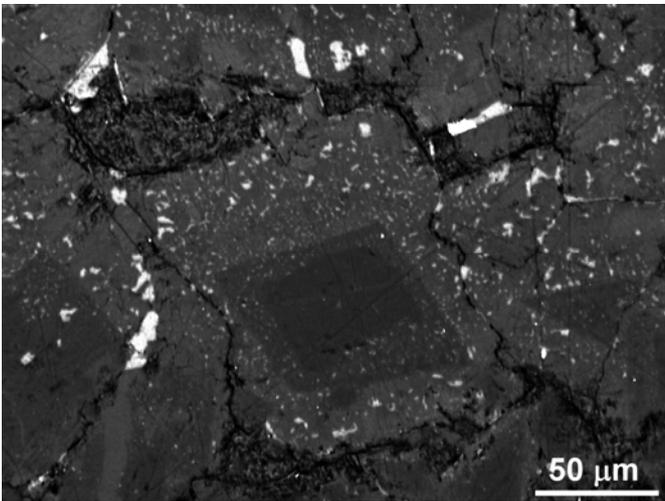668   Fig. 7

669

670

671

672   Fig. 8

673

674

675

676   Fig. 9

677
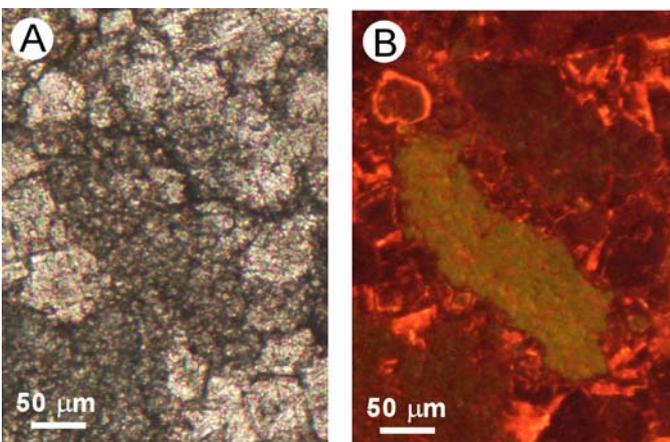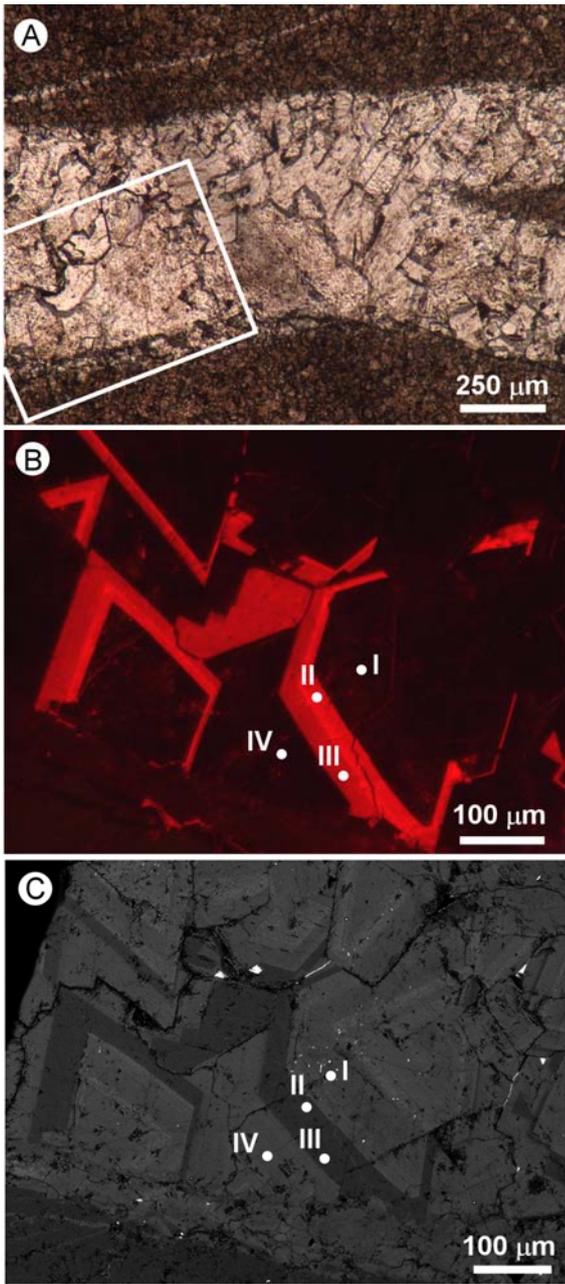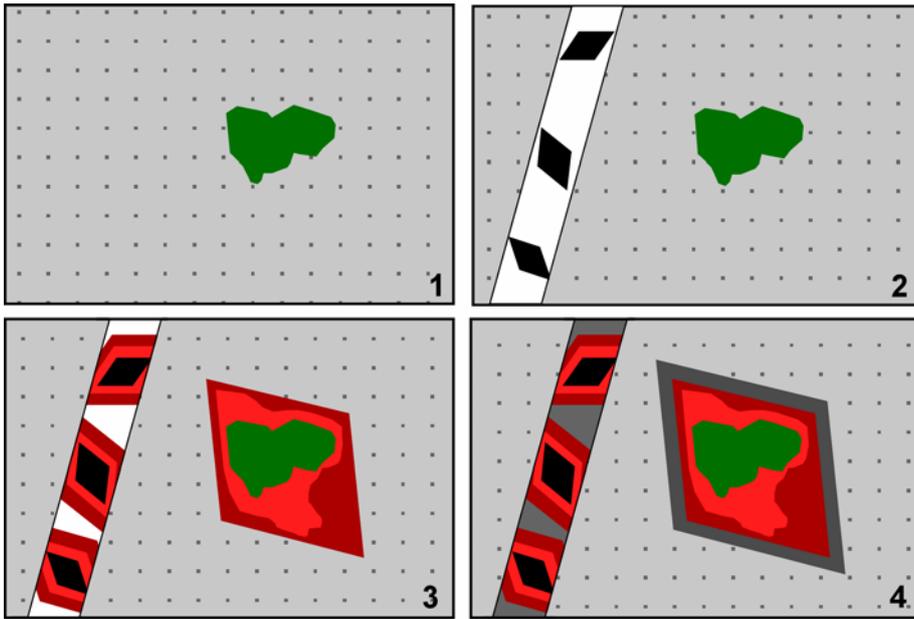

678

679   Fig. 10

680

681

682

683   Fig. 11

684

685

686   Fig. 12

687

688

689   Fig. 13